Nanoscale

PAPER

View Article Online
View Journal | View Issue

Cite this: *Nanoscale*, 2025, **17**, 8892

Organic electrochemical transistors based on a conjugated diketopyrrolopyrrole-dialkoxybithiazole copolymer†

Zilan Chen,[a] Xiaowei Zhao,[a] Chengdong Wang,[a] Wenxin Fang,[a] Gang Ye, *[b] Lichuan Chen,[c] Junyu Li[d] and Yanxi Zhang *[a]

Received 26th January 2025,
Accepted 4th March 2025

DOI: 10.1039/d5nr00379b

rsc.li/nanoscale

Organic electrochemical transistors (OECTs) are promising for bioelectronics due to their ability to amplify signals by converting ionic signals into electronic signals. The performance of OECTs relies heavily on the interaction between electrolyte ions and organic mixed ionic-electronic conductors (OMIECs). We examined how different aqueous electrolytes affect OECTs based on an ethylene glycol-substituted diketopyrrolopyrrole-dialkoxybithiazole copolymer (PDPP-TEG-2Tz), which is primarily p-type and electrochemically doped with anions. Our findings show that compared to the small, highly hydrated chloride anion (Cl^-), the larger hexafluorophosphate (PF_6^-) and bis(trifluoromethanesulfonyl)imide ($TFSI^-$) anions result in a lower threshold voltage and a faster transient response. Cations like Li^+, Na^+, and K^+ have little impact on OECT performance. Additionally, we created a complementary inverter using p-type PDPP-TEG-2Tz with an n-type naphthalene diimide-bithiophene copolymer (PNDI2C8TEG-2T), achieving a maximum voltage gain of 22.6 at a supply voltage of 0.7 V.

1. Introduction

Organic electrochemical transistors (OECTs) are pivotal in bioelectronics and printed electronics, with applications spanning neural interfaces,[1–3] sensors,[4,5] printed circuits,[6,7] and neuromorphic computing.[8–10] An OECT consists of source, drain, and gate electrodes, along with a film made of organic mixed ionic-electronic conductors (OMIECs), and an electrolyte.[11] OMIECs have the unique capability to conduct both ions and electrons, allowing them to effectively convert ionic signals into electrical signals.[12] The operation of an OECT involves a gate voltage (V_G) that drives ions into the OMIEC channel, leading to electrochemical doping. When exposed to aqueous electrolytes, the organic film undergoes hydration and microstructural changes, significantly impacting its morphology and the device performance.[13] The penetration of ions transforms the film's microscopic structure, a process that is complex and influenced by the type of electrolyte used.[14]

Understanding the electrochemical doping mechanism in OMIECs is essential for optimizing OECT performance. Research has shown that the size of anions plays a critical role in determining OECT characteristics. For instance, findings by Ginger *et al.* indicated that larger anions such as PF_6^- and $TFSI^-$ enhance source–drain currents and lower threshold voltages in homo-thiophene (P3HT)-based OECTs when compared to smaller anions like fluoride or chloride.[14] Similarly, Rivnay *et al.* demonstrated that larger, less hydrated anions could improve the transconductance of the donor-type polymer Pg2T-TT, though at the cost of slower switching speeds.[15] Aetukuri *et al.* reported that in an all-acceptor type homo-diketopyrrolopyrrole-based ambipolar conjugated polymer, the dependence of ion insertion on charge polarity resulted in increased p-type source–drain currents as the ionic radii of the anions increased.[16]

These research groups collectively observed that larger anions lead to higher source–drain currents and lower threshold voltages in OECT devices. Nevertheless, the trend still needs to be clarified in donor–acceptor (D–A) type conjugated polymers, which avoid non-capacitive faradaic side reactions by adjusting frontier molecular orbitals, thus preventing the formation of reactive side products and enhancing OECT stability.[17] Evaluating how anion size affects the performance

[a]*Institute of Flexible Electronics (IFE, Future Technologies), Xiamen University, Xiamen 361005, China. E-mail: ifeyxzhang@xmu.edu.cn*
[b]*Key Laboratory for the Green Preparation and Application of Functional Materials, Hubei Key Laboratory of Polymer Materials, School of Materials Science and Engineering, Hubei University, Youyi Road 368, Wuhan, 430062 China. E-mail: g.ye0612@hubu.edu.cn*
[c]*State Key Laboratory of Physical Chemistry of Solid Surfaces, College of Chemistry and Chemical Engineering, Xiamen University, Xiamen 361005, China*
[d]*Sinopec Shanghai Research Institute of Petrochemical Technology, Shanghai 201028, China*

† Electronic supplementary information (ESI) available. See DOI: https://doi.org/10.1039/d5nr00379b

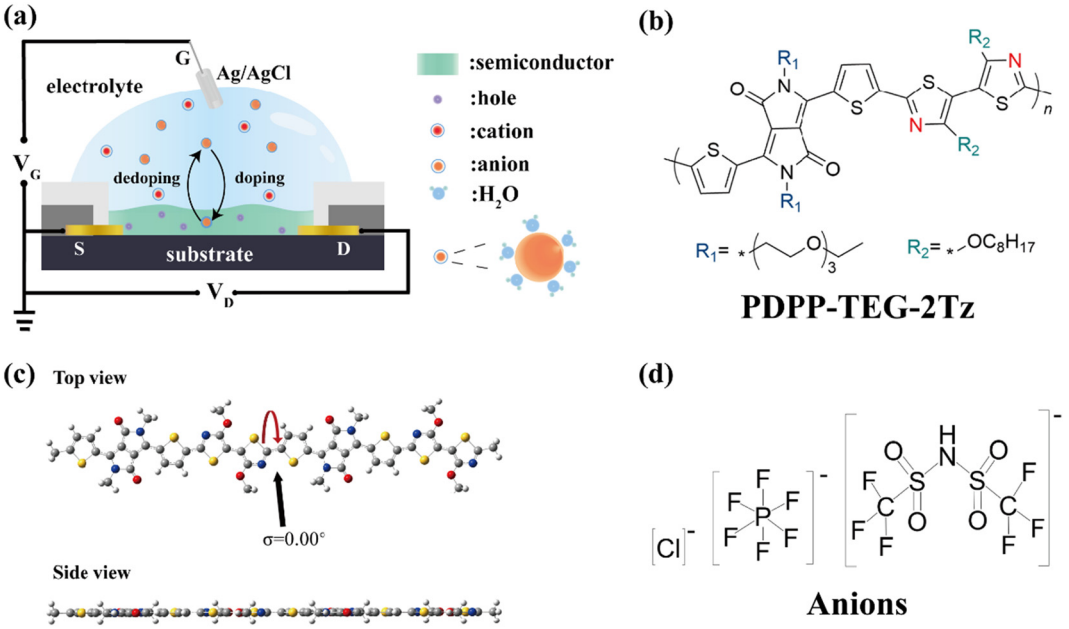

Fig. 1 (a) Schematic diagram of the OECT device architecture. Cations are represented in red, anions in orange, and the hydrated shell around the ions is depicted in light blue. (b) Molecular structure of the PDPP-TEG-2Tz copolymer. (c) Optimized molecular geometries of DPP-2Tz with two repeating units. (d) Chemical structures of anions used in this study, including chloride, hexafluorophosphate, and bis(trifluoromethanesulfonyl) imide.

of OECTs based on D–A polymers is essential for enhancing device operation.

In our study, we synthesized the conjugated polymer PDPP-TEG-2Tz, incorporating diketopyrrolopyrrole (DPP) and thiazole (Tz) moieties. DPP was chosen as the electron-deficient moiety because of its high mobility in solid-state films, attributed to dense π–π stacking and a planar backbone.[18–21] Building on our previous findings,[22–24] we combined the weak electron donor dialkoxybithiazole (2Tz) moiety[25–27] with the compact DPP to create a planar and rigid D–A structure. It is worth mentioning that DPP and Tz act as acceptors relative to the thiophene unit. Therefore, the polymer can also be regarded as dual-A.[18,28,29] We evaluated PDPP-TEG-2Tz OECTs (Fig. 1a) using various electrolytes and discovered that larger, polarizable anions like PF_6^- and $TFSI^-$ reduce the threshold voltage compared to smaller ions like Cl^-, which is consistent with a previous study on P3HT OECTs.[14] We utilized grazing incidence wide-angle X-ray scattering (GIWAXS) to characterize film morphology and conducted cyclic voltammetry (CV) and electrochemical spectroscopy to gain insights into the doping process. Finally, we paired p-type PDPP-TEG-2Tz with n-type PNDI2C8TEG-2T to create a complementary inverter.

2. Experimental

2.1 Materials

The synthesis of PDPP-TEG-2Tz is detailed in the ESI.† The polymer PNDI2C8TEG-2T was synthesized according to the literature.[29] 4,4′-Bis(octyloxy)-2,2′-bis(trimethylstannyl)-5,5′-bithiazole (2Tz) was purchased from SunaTech. Lithium chloride (LiCl), sodium chloride (NaCl), and potassium chloride (KCl) were purchased from Shanghai Titan Technology Co., Ltd. Lithium hexafluorophosphate ($LiPF_6$), sodium hexafluorophosphate ($NaPF_6$), potassium hexafluorophosphate (KPF_6), sodium bis(trifluoromethanesulfonyl)imine (NaTFSI) and potassium bis(trifluoromethanesulfonyl)imine (KTFSI) were purchased from Suzhou Duoduo Chemical Technology Co., Ltd. Lithium bis(trifluoromethanesulfonyl)imine (LiTFSI) was purchased from Shanghai Aladdin Biochemical Technology Co., Ltd. Chloroform ($CHCl_3$) was supplied by Sinopharm Group Co., Ltd. 1-Ethyl-3-methylimidazolium bis(trifluorosulfonyl)imide (EMIM:TFSI) was purchased from Qingdao Aolike Company. Poly(vinylidene fluoride-*co*-hexafluoropropylene) (PVDF-HFP) was purchased from Shanghai Maclin Company. The interdigitated microelectrodes (ED-IDA6-Au) were purchased from MicruX Technologies (30 pairs, channel length: 5 micrometers, and individual channel width: 1.8 millimeters).

2.2 Device fabrication and characterization

In order to fabricate OECT devices using a p-type polymer – PDPP-TEG-2Tz and an n-type polymer – PNDI2C8TEG-2T, the polymers are dissolved in chloroform to form a 5 mg mL^{-1} solution. The microelectrodes are cleaned with ultraviolet ozone for 30 minutes. This is followed by spin-coating the polymer solution at 1000 rpm for 30 seconds and then annealing the coated electrodes on a hot plate set to 100 °C for 30 minutes. When using ion gel as the electrolyte, the ionic liquid (EMIM:TFSI) and poly(vinylidene fluoride-*co*-hexafluoropropylene) are mixed in acetone with specific weight pro-

portions: 17.6% ionic liquid, 4.4% polymer, and 78% solvent. This mixture is then stirred at 40 °C for a minimum of 30 minutes to ensure proper dissolution and homogenization of the components, resulting in the ion gel solution. The ion gel solution is deposited onto the active area *via* drop-casting and subsequently air-dried in a fume hood.

The characterization of OECTs based on PDPP-TEG-2Tz and PNDI2C8TEG-2T includes transfer and output curves, cycling stability, and transient response. These measurements were conducted using a Keithley 2612B digital source meter with a self-custom LabVIEW program. The transient response was measured using a Keysight B2912B source meter.

A Keithley 2450 in combination with NI4140 and NI4183 was employed along with a self-developed LabVIEW program for the inverter characterization.

2.3 Polymer thin film characterization

Cyclic voltammetry (CV): cyclic voltammetry experiments were performed using a Shanghai Chenhua CHI 600E electrochemical analyzer in various aqueous electrolyte solutions at a concentration of 0.1 M. The working electrode, made of ITO, was coated with the polymer, while a platinum sheet served as the counter electrode, and an Ag/AgCl electrode acted as the reference electrode. CV testing covered a voltage range from 0 V to 0.9 V, with a scanning speed of 100 mV s^{-1}.

Electrochemical spectroscopy: electrochemical spectroscopy was performed by using a Shimadzu UV-190i and an electrochemical workstation. A polymer solution with a concentration of 5 mg mL^{-1} was spin-coated onto an ITO surface at 1000 rpm for 30 seconds. The coated ITO was the working electrode and immersed in different 0.1 M aqueous electrolyte solutions. An Ag/AgCl electrode was used as both the reference and counter electrodes. Before testing, a background measurement was conducted using a clean ITO substrate.

Grazing incidence wide angle X-ray scattering (GIWAXS): GIWAXS experiments were carried out using the Xeuss 3.0 UHR system from Xenocs. The instrument is equipped with an Eiger 500 K detector with a pixel size of 75 μm × 75 μm. The X-ray source is a microfocus sealed tube X-ray Cu-source with a wavelength of λ = 1.54 Å. The sample was placed vertically on a goniometer at a grazing angle of 0.2° relative to the incident beam. The sample to detector distance (SDD) was 75 mm. Each measurement had an accumulation time of 20 min.

Film thickness measurement: the film thickness measured using an atomic force microscope (AFM, Bruker Nano instrument) was found to be 28.2 nm.

Water contact angle measurement: contact angle measurements were performed using a Guangdong Beidou Precision Instrument CA500.

3. Results and discussion

3.1. Materials synthesis

The molecular structure of PDPP-TEG-2Tz is presented in Fig. 1b and the synthetic route is provided in Scheme S1.† The dibrominated monomer DPP-TEG-2Br was synthesized and purified according to the literature.[29,30] The D–A type polymer PDPP-TEG-2Tz was synthesized by the palladium-catalyzed Stille coupling polymerization of a symmetrical dibromo DPP monomer (DPP-TEG-2Br) and distannyl bithiazole monomers (2Tz). After polymerization, the impurities and low-molecular-weight fraction were removed by continuous extraction with hot methanol, followed by hexane and chloroform in a Soxhlet extractor. The final chloroform fraction was collected and reprecipitated into methanol and collected, and then dried *in vacuo* to afford the product polymer. The structures were then characterized by ^{1}HNMR and FTIR (Fig. S1 and S2, ESI†). The molecular weight of PDPP-TEG-2Tz was characterized by gel permeation chromatography (GPC) and the results are provided in Fig. S3.†

The lowest unoccupied molecular orbital (LUMO) and highest occupied molecular orbital (HOMO) levels of PDPP-TEG-2Tz were investigated using cyclic voltammetry in 0.1 M tetrabutylammonium hexafluorophosphate acetonitrile solution using a ferrocene/ferrocenium (Fc/Fc^+) redox couple as the external reference. From the reduction/oxidation onsets of the CV curve (Fig. S4†), the LUMO/HOMO levels of PDPP-TEG-2Tz were calculated to be −3.76 eV and −5.03 eV. The optimized geometry of PDPP-TEG-2Tz adopted a planar structure with a dihedral angle of 0.00° (shown in Fig. 1c), which is beneficial for charge transport. The LUMO and HOMO were −3.10 and −4.71 eV, calculated using density functional theory (TD-DFT/B3LYP/6-311G(d,p)).

3.2. OECT characterization

We investigated the p-type operation of OECTs based on PDPP-TEG-2Tz in nine different aqueous electrolytes, each with a concentration of 0.1 M, including three different types of anions (Fig. 1d). When tested in the widely used 0.1 M NaCl aqueous electrolyte, the transistor exhibits an on–off ratio exceeding 10^3 and a transconductance of approximately 79.85 ± 24.41 mS. The transistor's transfer curves are useful for a more detailed comparison of the impacts of different electrolytes. Fig. 2 illustrates that while the various cations (Li^+, Na^+ and K^+) have minimal impact on the device's performance (a–c), the choice of anions (Cl^-, PF_6^- and $TFSI^-$) significantly influences the transfer curves of OECTs (d–f). The maximum transconductance (g_m) is attained at lower gate voltages (V_G) when larger anions, such as $TFSI^-$, are used.

The results and comparisons of OECT measurements, including transfer and output curves, in the different electrolytes can be found in Fig. S5–8.† To ensure the reliability of the findings, reproducibility tests, shown in Fig. S9,† were conducted using at least seven different OECT devices for each electrolyte. This approach helps to rule out the effects of a single experiment and provides a more robust assessment of the performance. The shapes of the transfer curves show similarity for a given anion and are independent of the cation. The statistical analysis indicates that the on-currents obtained in PF_6^- and $TFSI^-$ are not significantly higher than those in Cl^-, as illustrated in Fig. S12(d–f).† Fig. 3(a–c) present the

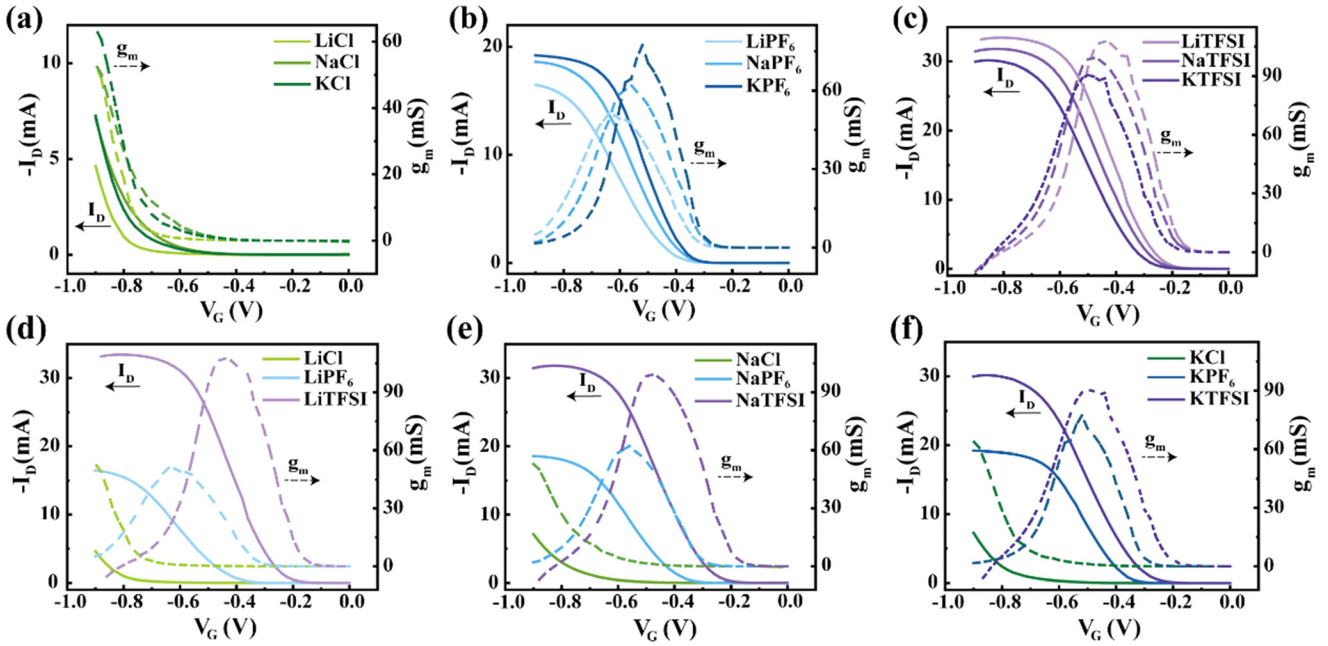

Fig. 2 The transfer characteristics of OECTs with different electrolytes. The solid lines represent the transfer curves and the dashed lines represent the transconductance. (a–c) Electrolytes with a concentration of 0.1 M that contain different cations (Li^+, Na^+ and K^+) while maintaining the same anion. (d–f) Electrolytes with a concentration of 0.1 M that contain different anions (Cl^-, PF_6^- and $TFSI^-$) while maintaining the same cation.

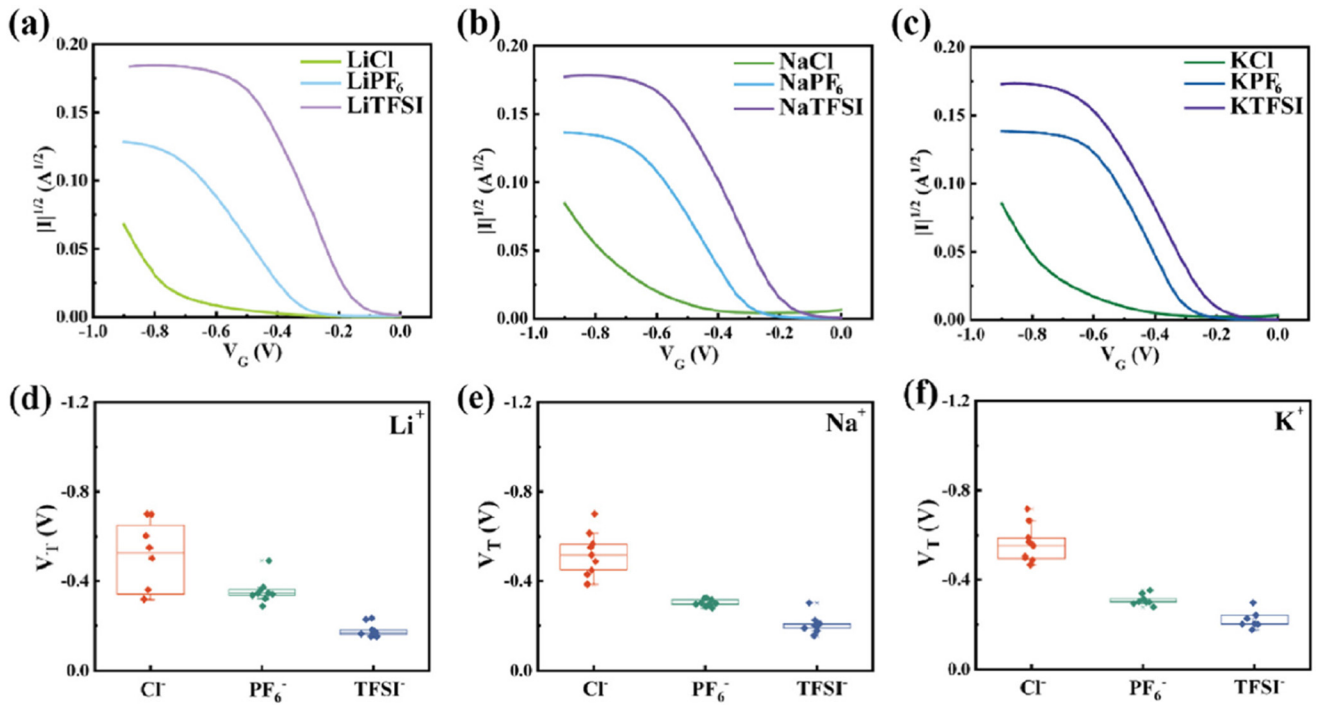

Fig. 3 The threshold voltage (V_T) of OECTs with different electrolytes. (a–c) V_T is extracted from the transfer curve by finding the x-axis intercept using $\sqrt{I_D}$ as a function of V_G. (d–f) Comparison of electrolytes containing the same cation but different anions (Cl^-, PF_6^- and $TFSI^-$). Each point represents an individual OECT. For box plots, the center line is the median; box limits are 25th and 75th percentiles; whiskers are outliers within the 25th and 75th percentiles + 1.5× the interquartile range; "□" is the average; "x" represents the maximum and minimum values.

threshold voltage (V_T) of OECTs with different electrolytes, plotting $|I|^{1/2}$ against V_G. These figures highlight the notable variations in V_T resulting from different anions. To address the potential device-to-device variation, a statistical analysis was conducted. Fig. 3(d–f) show box plots that represent the V_T measured for the OECTs containing the same cation but

different anions. The data indicate that Cl^- results in a higher threshold voltage compared to the other tested anions, PF_6^- and $TFSI^-$. The threshold voltage follows the order: Cl^- > PF_6^- > $TFSI^-$. Additionally, the turn-on transient response time (τ_{on}) exhibits the same order, as shown in Fig. S15.†

The larger, hydrophobic ions $TFSI^-$ and PF_6^- have lower hydration numbers compared to Cl^-. Consequently, the energy required for these ions to move from water into the polymer differs significantly. Additionally, since $TFSI^-$ and PF_6^- are more hydrophobic, they are likely to be more stable within a polymer matrix than in water. This leads to more favorable interactions between the polymer and these anions compared to Cl^-. These two energetic factors could contribute to the differences in the injection barrier and kinetics by altering the doping activation energy, which in turn affects the threshold voltage and transient response.[14]

In several studies, including our own, it has been noted that larger chaotropic ions such as $TFSI^-$ and PF_6^-, which have lower surface charge densities, can more easily penetrate the polymer active layer and dope the polymer to higher levels compared to smaller kosmotropic ions like Cl^-, which have high surface charge densities. This observation applies regardless of the side-chain functionality and polymer backbones and represents a general principle in the operation of OECTs. The maximum transconductance and the on–off ratio exhibit no significant difference. A more detailed comparison of the parameters is available in Fig. S10–14.† Additionally, we assessed the device stability when operated in different electrolytes by applying continuous voltage pulses. We found that the stability is also dependent on the anion (see Fig. S16†). The devices operated in PF_6^- and $TFSI^-$ retain a higher percentage of on-current than Cl^- after on–off switching cycles, as seen in Fig. S17.† Thus, we hypothesize that the chaotropic anions with lower hydration cause less damage to the polymer film's morphology during electrochemical doping, resulting in better operational stability. A summary of the OECT performance in different electrolytes is provided in Table S1.†

3.3. Characterization of polymer films

The charge mobility of organic semiconductors is greatly influenced by the transport pathways, which are determined by the molecular packing and the orientation of stacking.[31] To analyze the microscopic morphology and molecular packing of the PDPP-TEG-2Tz film, grazing-incidence wide-angle X-ray scattering (GIWAXS) was employed. The two-dimensional GIWAXS patterns in the PDPP-TEG-2Tz film are depicted in Fig. 4a. In the out-of-plane (OPP) direction, the diffraction ring of the PDPP-TEG-2Tz film appears narrowed, forming high-density spots. Distinct diffraction peaks at q_z = 0.38 $Å^{-1}$ and 0.71 $Å^{-1}$ are observed, corresponding to the (100) and (200) crystal planes, respectively (Fig. 4b). This suggests that the polymers are in an edge-on orientation. In the in-plane (IP) direction, no π–π stacking diffraction peaks were observed (Fig. 4c). Additionally, we used the Scherrer formula (CL = $K\lambda/\beta\cos(\theta)$) to determine the coherent domain size and polycrystalline disorder factor (g = SQRT(FWHM/$2\pi q$)), as shown in ESI Table S2.† This analysis, considering the low solubility of PDPP-TEG-2Tz leading to poor film morphology, was crucial for understanding its impact on OECT performance.

During the cyclic voltammetry (CV) test, the voltage is measured from 0 to 0.9 V relative to Ag/AgCl, as illustrated in Fig. 5(a–c). In the forward scan, the polymer undergoes oxidation while anions are inserted. Subsequently, during the reverse scan, the polymer film returns to its neutral state, and the anions are expelled. The oxidation of PDPP-TEG-2Tz in different electrolytes implies that it is a p-type polymer. Its oxidation peaks are observed in the forward scan, with the corresponding reduction peak appearing in the reverse scan. These results demonstrate that the process of doping and dedoping of anions is reversible. We calculated the oxidation onset potential (V_{ox}) of the polymer in various electrolytes from the CV curves, as shown in Fig. S19.† The CV curves appear similar when the cations are varied, but the influence of anions is noteworthy. The onset potential decreases in the following order: Cl^- > PF_6^- > $TFSI^-$. This observed trend correlates with the threshold voltage of OECTs. The CV results further substantiate that the electrochemical doping of p-type polymers is determined by anion insertion. The anion $TFSI^-$, having less solvation, exhibits a lower threshold voltage, an earlier doping onset, and faster transient kinetics.

Next, we conducted electrochemical spectroscopy to analyze changes in the optical properties of the PDPP-TEG-2Tz film in nine electrolytes upon electrochemical doping at a concentration of 0.1 M each. The evolution of the relative absorption

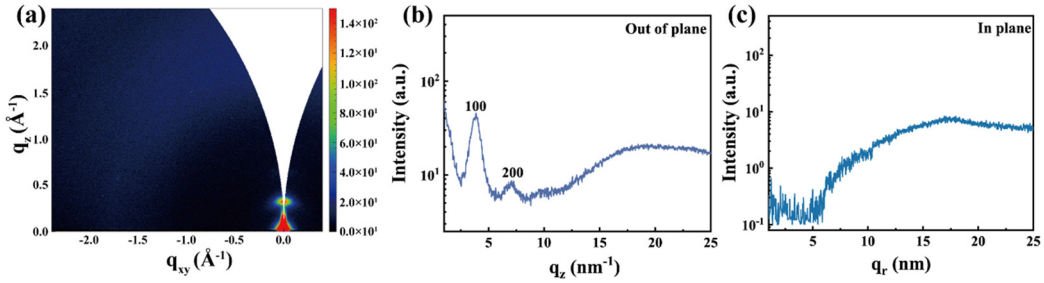

Fig. 4 GIWAXS analysis. (a) 2D GIWAXS pattern. (b) Out of plane (q_z) and (c) in plane (q_r) orientation integrations of PDPP-TEG-2Tz, as derived from 2D GIWAXS.

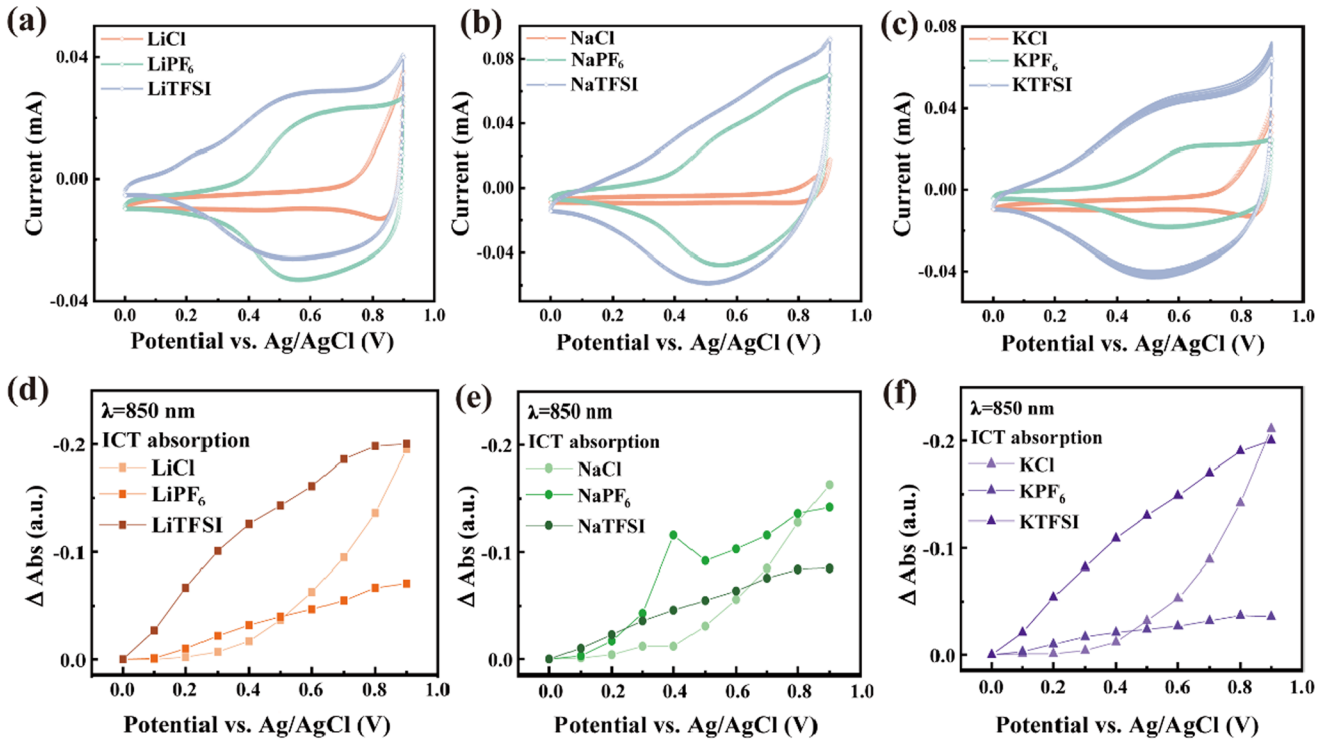

Fig. 5 Cyclic voltammetry (CV) and electrochemical spectroscopy in aqueous electrolyte. (a–c) 10 CV cycles at a scan rate of 100 mV s^{-1}, starting from 0 to 0.9 V. (d–f) The evolution of the relative absorption at 850 nm (ICT) as the potential increases.

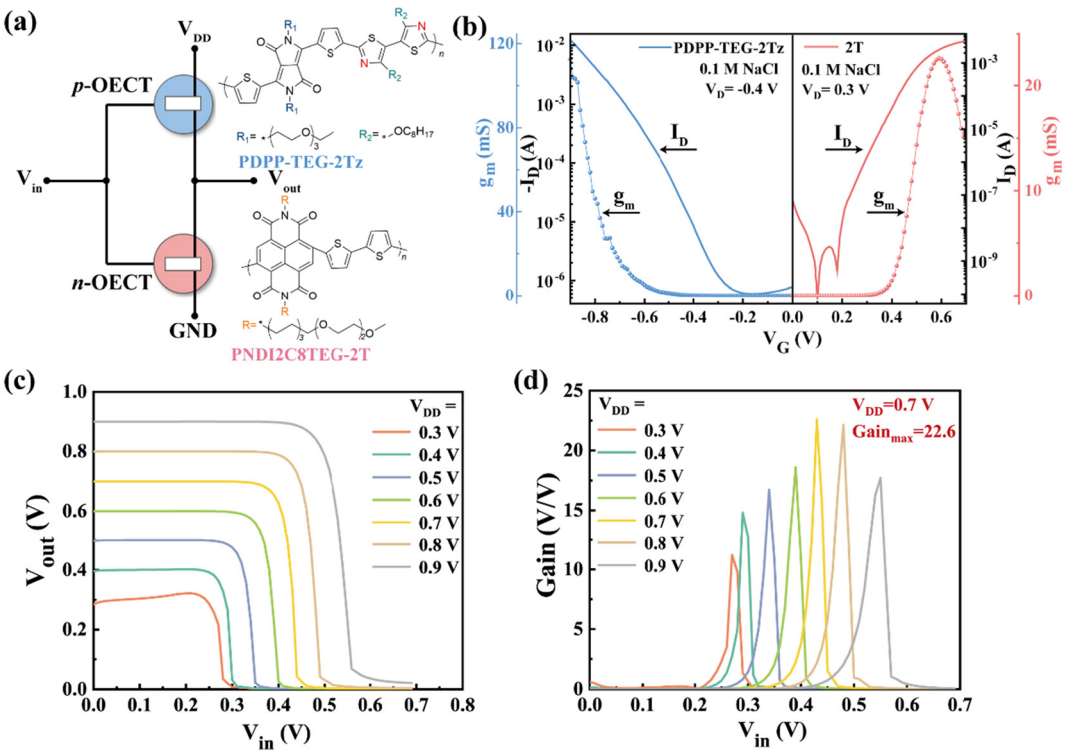

Fig. 6 OECT-based complementary inverter. (a) Schematic diagram for the complementary inverter, which utilizes PDPP-TEG-2Tz (p-type) and PNDI2C8TEG-2T (n-type) as channel materials. The chemical structures of these materials are shown. (b) The transfer curves of the OECTs based on PDPP-TEG-2Tz and PNDI2C8TEG-2T, along with their corresponding transconductances, indicating that the p-type and n-type properties are relatively balanced. (c) The voltage transfer characteristics of the inverter at varying supply voltages, ranging from 0.3 to 0.9 V. (d) The corresponding voltage gain ($\partial V_{out}/\partial V_{in}$) of the inverter at different supply voltages.

spectra with positive bias, ΔAbs (relative to the spectrum obtained at 0 V), for the nine electrolytes is depicted in Fig. S20.† PDPP-TEG-2Tz exhibits a broad absorption spectrum with a peak at 850 nm, and this absorption is attributed to intramolecular charge transfer (ICT). In Fig. 5d–f, the changes in relative absorption at 850 nm with a positive bias are presented. It is observed that ΔAbs (*y*-axis) becomes increasingly negative as the bias is increased. The bleaching behavior indicates that the volume oxidation takes place, showing that the electrolyte can penetrate the entire film, leading to the oxidation of the polymers. As a result, this process reduces the absorption in the visible range. This observation aligns with previous findings in DPP-type polymers.[17] Our instrument's detection limits prevent us from observing the formation of polarons and bipolarons, which typically absorb much higher wavelengths (>1100 nm).

3.4. Complementary inverters

OECT-based complementary inverters have recently attracted attention due to their potential applications in logic circuits and amplification[32] of electrophysiology signals.[33] When creating a complementary inverter, both p-type and n-type OECT devices are typically required. In our approach, we selected an n-type semiconducting polymer, PNDI2C8TEG-2T, known for its balanced transistor characteristics, and paired it with a p-type OECT based on PDPP-TEG-2Tz to demonstrate a practical application scenario (Fig. 6a). The n-type OECT exhibited a threshold voltage of 0.40 V, a switching ratio exceeding 10^5, and a transconductance of 22.61 mS, complementing the characteristics of the p-type OECT (Fig. 6b and S22†). These well-balanced p-type and n-type electrical properties enable the inverter to operate at supply voltages as low as 0.3 V (V_{DD}), achieving a voltage gain of over 10 V/V and reaching a maximum gain of 22.6 V/V at 0.7 V (Fig. 6c and d). To further optimize OECTs, varying molecular weights and alkyl chain lengths will be considered, as these parameters will affect the doping efficiency, swelling, and molecular packing.[23,34,35]

4. Conclusion

In our research, we developed a donor–acceptor (D–A) conjugated polymer called PDPP-TEG-2Tz, synthesized by copolymerizing diketopyrrolopyrrole (DPP) with dialkoxybithiadiazole (2Tz) units. We studied the polymer's properties as an OECT active layer and looked into how the electrochemical doping process is affected by different ions. Our analysis revealed that large, chaotropic anions like $TFSI^-$ and PF_6^-, which have less hydration, lead to lower threshold voltages and earlier doping onsets and faster transient turn-on times than small, kosmotropic anions like Cl^-. The presence of cations (Li^+, Na^+ and K^+) has a minimal effect on OECTs that are based on PDPP-TEG-2Tz. Additionally, complementary inverters made with this device have shown that the maximum voltage gain reaches 22.6 VV^{-1} at a V_{DD} of 0.7 V.

Data availability

The data supporting this article have been included as part of the ESI.†

Conflicts of interest

The authors declare that they have no conflict of interest.

Acknowledgements

We acknowledge financial support from the National Natural Science Foundation of China (No. 22303071) and the Fundamental Research Funds for the Central Universities (No. 20720240040).

References

1 D. Khodagholy, D. Thomas, Q. Pascale, G. Moshe, L. Pierre, G. Antoine, I. Esma, H. Thierry, S. Sébastien, B. Christophe and G. M. George, In Vivo Recordings of Brain Activity Using Organic Transistors, *Nat. Commun.*, 2013, **4**(1), 1575.
2 I. Uguz, D. Ohayon, S. Yilmaz, S. Griggs, R. Sheelamanthula, J. D. Fabbri, I. McCulloch, S. Inal and K. L. Shepard, Complementary Integration of Organic Electrochemical Transistors for Front-End Amplifier Circuits of Flexible Neural Implants, *Sci. Adv.*, 2024, **10**(12), eadi9710.
3 P. C. Harikesh, D. Tu and S. Fabiano, Organic Electrochemical Neurons for Neuromorphic Perception, *Nat. Electron.*, 2024, **7**, 525–536.
4 P. Lin and F. Yan, Organic Thin-Film Transistors for Chemical and Biological Sensing, *Adv. Mater.*, 2012, **24**(1), 34–51.
5 Y. Wang, S. Wustoni, J. Surgailis, Y. Zhong, A. Koklu and S. Inal, Designing Organic Mixed Conductors for Electrochemical Transistor Applications, *Nat. Rev. Mater.*, 2024, **9**, 249–265.
6 D. Nilsson, N. Robinson, M. Berggren and R. Forchheimer, Electrochemical Logic Circuits, *Adv. Mater.*, 2005, **17**(3), 353–358.
7 P. Andersson Ersman, R. Lassnig, J. Strandberg, D. Tu, V. Keshmiri, R. Forchheimer, S. Fabiano, G. Gustafsson and M. Berggren, All-Printed Large-Scale Integrated Circuits Based on Organic Electrochemical Transistors, *Nat. Commun.*, 2019, **10**(1), 5053.
8 P. Gkoupidenis, N. Schaefer, B. Garlan and G. G. Malliaras, Neuromorphic Functions in PEDOT:PSS Organic Electrochemical Transistors, *Adv. Mater.*, 2015, **27**(44), 7176–7180.
9 Y. van de Burgt, A. Melianas, S. T. Keene, G. Malliaras and A. Salleo, Organic Electronics for Neuromorphic Computing, *Nat. Electron.*, 2018, **1**(7), 386–397.

10 P. Gkoupidenis, Y. Zhang, H. Kleemann, *et al.*, Organic Mixed Conductors for Bioinspired Electronics, *Nat. Rev. Mater.*, 2024, **9**, 134–149.
11 J. Rivnay, S. Inal, A. Salleo, R. M. Owens, M. Berggren and G. G. Malliaras, Organic Electrochemical Transistors, *Nat. Rev. Mater.*, 2018, **3**(2), 17086.
12 B. D. Paulsen, K. Tybrandt, E. Stavrinidou and J. Rivnay, Organic Mixed Ionic-Electronic Conductors, *Nat. Mater.*, 2020, **19**(1), 13–26.
13 C. Cendra, A. Giovannitti, A. Savva, V. Venkatraman, I. McCulloch, A. Salleo, S. Inal and J. Rivnay, Role of the Anion on the Transport and Structure of Organic Mixed Conductors, *Adv. Funct. Mater.*, 2019, **29**(5), 1807034.
14 L. Q. Flagg, R. Giridharagopal, J. Guo and D. S. Ginger, Anion-Dependent Doping and Charge Transport in Organic Electrochemical Transistors, *Chem. Mater.*, 2018, **30 (15)**, 5380–5389.
15 A. Giovannitti, R. B. Rashid, Q. Thiburce, B. D. Paulsen, C. Cendra, K. Thorley, D. Moia, J. T. Mefford, D. Hanifi, D. Weiyuan, M. Moser, A. Salleo, J. Nelson, I. McCulloch and J. Rivnay, Energetic Control of Redox-Active Polymers toward Safe Organic Bioelectronic Materials, *Adv. Mater.*, 2020, **32**(16), 1908047.
16 J. J. Samuel, A. Garudapalli, C. Gangadharappa, S. R. Mahapatra, S. Patil and N. P. B. Aetukuri, Charge Polarity-Dependent Ion-Insertion Asymmetry during Electrochemical Doping of an Ambipolar π-Conjugated Polymer, *Nat. Commun.*, 2022, **13**(1), 7788.
17 L. Q. Flagg, C. G. Bischak, J. W. Onorato, R. B. Rashid, C. K. Luscombe and D. S. Ginger, Polymer Crystallinity Controls Water Uptake in Glycol Side-Chain Polymer Organic Electrochemical Transistors, *J. Am. Chem. Soc.*, 2019, **141 (10)**, 4345–4354.
18 Y. H. Zhao, W. Li, T. Shen, Y. Zhao, Y. Liu and Y. Wang, The Marriage of Dual-Acceptor Strategy and C-H Activation Polymerization: Naphthalene Diimide-Based n-Type Polymers with Adjustable Molar Mass and Decent Performance, *Sci. China: Chem.*, 2023, **66**(2), 548–561.
19 L. Yang, S. Shen, X. Chen, H. Wei, D. Xia, C. Zhao, N. Zhang, Y. Hu, W. Li, H. Xin and J. Song, Doped/Undoped A1−A2 Typed Copolymers as ETLs for Highly Efficient Organic Solar Cells, *Adv. Funct. Mater.*, 2023, **33**(36), 2303603.
20 H. Jia, Z. Huang, P. Li, S. Zhang, Y. Wang, J. Y. Wang, X. Gu and T. Lei, Engineering Donor–Acceptor Conjugated Polymers for High-Performance and Fast-Response Organic Electrochemical Transistors, *J. Mater. Chem. C*, 2021, **9**(14), 4927–4934.
21 Y. Zhang, E. R. W. van Doremaele, G. Ye, T. Stevens, J. Song, R. C. Chiechi and Y. van de Burgt, Adaptive Biosensing and Neuromorphic Classification Based on an Ambipolar Organic Mixed Ionic-Electronic Conductor, *Adv. Mater.*, 2022, **34**(20), 2200393.
22 Y. Zhang, G. Ye, T. P. A. Van Der Pol, J. Dong, E. R. W. Van Doremaele, I. Krauhausen, Y. Liu, P. Gkoupidenis, G. Portale, J. Song, R. C. Chiechi and Y. Van De Burgt, High-Performance Organic Electrochemical Transistors and Neuromorphic Devices Comprising Naphthalenediimide-Dialkoxybithiazole Copolymers Bearing Glycol Ether Pendant Groups, *Adv. Funct. Mater.*, 2022, **32**(27), 2201593.
23 T. Pan, X. Jiang, E. R. W. Van Doremaele, J. Li, T. P. A. Van Der Pol, C. Yan, G. Ye, J. Liu, W. Hong, R. C. Chiechi, Y. V. De Burgt and Y. Zhang, Over 60 h of Stable Water-Operation for N-Type Organic Electrochemical Transistors with Fast Response and Ambipolarity, *Adv. Sci.*, 2024, 2400872.
24 D. Ohayon, A. Savva, W. Du, B. D. Paulsen, I. Uguz, R. S. Ashraf, J. Rivnay, I. McCulloch and S. Inal, Influence of Side Chains on the *n*-Type Organic Electrochemical Transistor Performance, *ACS Appl. Mater. Interfaces*, 2021, **13**(3), 4253–4266.
25 B. Ma, Q. Shi, X. Ma, Y. Li, H. Chen, K. Wen, R. Zhao, F. Zhang, Y. Lin, Z. Wang and H. Huang, Defect-Free Alternating Conjugated Polymers Enabled by Room-Temperature Stille Polymerization, *Angew. Chem., Int. Ed.*, 2022, **61**, e202115969.
26 K. Yang, Z. Chen, Y. Wang and X. Guo, Alkoxy-Functionalized Bithiophene/Thiazoles: Versatile Building Blocks for High-Performance Organic and Polymeric Semiconductors, *Acc. Mater. Res.*, 2023, **4**(3), 237–250.
27 X. Guo, J. Quinn, Z. Chen, H. Usta, Y. Zheng, Y. Xia, J. W. Hennek, R. P. Ortiz, T. J. Marks and A. Facchetti, Dialkoxybithiazole: A New Building Block for Head-to-Head Polymer Semiconductors, *J. Am. Chem. Soc.*, 2013, **135**(5), 1986–1996.
28 L. Yang, S. Shen, X. Chen, H. Wei, D. Xia, C. Zhao, N. Zhang, Y. Hu, W. Li, H. Xin and J. Song, Doped/Undoped A1-A2 Typed Copolymers as ETLs for Highly Efficient Organic Solar Cells, *Adv. Funct. Mater.*, 2023, **33**, 2303603.
29 J. Mei, K. R. Graham, R. Stalder, S. P. Tiwari, H. Cheun, J. Shim, M. Yoshio, C. Nuckolls, B. Kippelen, R. K. Castellano and J. R. Reynolds, Self-Assembled Amphiphilic Diketopyrrolopyrrole-Based Oligothiophenes for Field-Effect Transistors and Solar Cells, *Chem. Mater.*, 2011, **23**(9), 2285–2288.
30 C. Kanimozhi, N. Yaacobi-Gross, K. W. Chou, A. Amassian, T. D. Anthopoulos and S. Patil, Diketopyrrolopyrrole-Diketopyrrolopyrrole-Based Conjugated Copolymer for High-Mobility Organic Field-Effect Transistors, *J. Am. Chem. Soc.*, 2012, **134**(40), 16532–16535.
31 S. Samal, H. Roh, C. E. Cunin, G. G. Yang and A. Gumyusenge, Molecularly Hybridized Conduction in DPP–Based Donor-Acceptor Copolymers toward High-Performance Iono-Electronics, *Small*, 2023, **19**(18), 2207554.
32 H. Sun, M. Vagin, S. Wang, X. Crispin, R. Forchheimer, M. Berggren and S. Fabiano, Complementary Logic Circuits Based on High-Performance *n*-Type Organic Electrochemical Transistors, *Adv. Mater.*, 2018, **30**(9), 1704916.

33 X. Wu, Q. He, Z. Zhou, T. L. D. Tam, C. Tang, M. Lin, M. Moser, S. Griggs, A. Marks, S. Chen, J. Xu, I. McCulloch and W. L. Leong, Stable *n*-Type Perylene Derivative Ladder Polymer with Antiambipolarity for Electrically Reconfigurable Organic Logic Gates, *Adv. Mater.*, 2024, 2308823.
34 H. Y. Wu, C. Y. Yang, Q. Li, N. B. Kolhe, X. Strakosas, M. A. Stoeckel, Z. Wu, W. Jin, M. Savvakis, R. Kroon, D. Tu, H. Y. Woo, M. Berggren, S. A. Jenekhe and S. Fabiano, Influence of Molecular Weight on the Organic Electrochemical Transistor Performance of Ladder-Type Conjugated Polymers, *Adv. Mater.*, 2022, **34**(2), 2106235.
35 Y. Kuang, S. Heester, S. Shao, G. Ye, T. Yao, Z. Xie, L. J. A. Koster and J. Liu, Adjusting Molecular Weight Optimizes Electronic Transport of Extrinsically N-Type Doped Conjugated Polymer Incorporating Glycolated Side Chains, *J. Mater. Chem. A*, 2024, **12**, 4866–4876.